A&A 613, A3 (2018)
https://doi.org/10.1051/0004-6361/201731035

Astronomy & Astrophysics

Deep millimeter spectroscopy observations toward NGC 1068⋆

Jianjie Qiu[1,2], Junzhi Wang[2,3], Yong Shi[1,4], Jiangshui Zhang[5], Min Fang[6], and Fei Li[2,7]

[1] School of Astronomy and Space Science, Nanjing University, Nanjing 210093, PR China
e-mail: qiujianjie2007@126.com
[2] Shanghai Astronomical Observatory, Chinese Academy of Sciences, 80 Nandan Road, Shanghai 200030, PR China
e-mail: jzwang@shao.ac.cn
[3] Key Laboratory of Radio Astronomy, Chinese Academy of Sciences, Nanjing 210008, PR China
[4] Key Laboratory of Modern Astronomy and Astrophysics, Nanjing University, Ministry of Education, Nanjing 210093, PR China
e-mail: yong@nju.edu.cn
[5] Center For Astrophysics, GuangZhou University, GuangZhou 510006, PR China
[6] Department of Astronomy, University of Arizona, 933 North Cherry Avenue, Tucson, AZ 85721, USA
[7] University of Chinese Academy of Sciences, 19A Yuquanlu, Beijing 100049, PR China

Received 25 April 2017 / Accepted 11 December 2017

ABSTRACT

Aims. We aim for a better understanding of gas properties in the circum-nuclear disk (CND) region of the nearby gas-rich Seyfert 2 galaxy NGC 1068. We focus on line identification and the basic physical parameters estimation of molecular gas in the CND region.
Methods. We used the IRAM 30 m telescope to conduct deep millimeter spectroscopy observations toward the center of NGC 1068.
Results. Thirty-two lines were detected in this galaxy, 15 lines of wich were detected for the first time. With a sensitivity better by about a factor of 4 than observations in the literature for this source at 3 mm band, we detected several weak lines for the first time in this source, such as lines from CH_3CCH, CH_3OCH_3, and $HC^{18}O^+$. Column densities of these molecules were estimated based on line emissions. Some marginal detections in the literature, such as $HN^{13}C$ (1–0), were confirmed. CH_3OCH_3 was detected for the first time in external galaxies. Lines from several carbon chain molecules and shock-related molecules were also detected in this source.

Key words. ISM: molecules – galaxies: ISM – galaxies: individual: NGC 1068 – galaxies: nuclei – galaxies: active

1. Introduction

As cold molecular clouds are opaque to the visible and UV radiation in the Milky Way and other galaxies, observations of molecular rotational transitions at millimeter wavelength are important to study the interstellar medium (ISM; Omont 2007). As a tracer of total molecular gas in galaxies, low-J CO transitions have been observed in more than one thousand galaxies (Sanders et al. 1991; Young & Scoville 1991; Kennicutt 1998), while lines of molecules with high dipole moments, such as HCN (1–0), have also been detected as dense gas tracers in many galaxies (Gao & Solomon 2004; Liu et al. 2015).

Multiple line observations, especially with lines of different molecules (Usero et al. 2004), can provide useful constraints on the gas properties. A broadband line survey toward nearby galaxies is a powerful tool for such a study, which has been performed for M82 (Aladro et al. 2011) and Arp 157 (Davis et al. 2013) at the 3 mm band, NGC 253 at the 2 mm band (Martín et al. 2006), and Arp 220 at the 1 mm band (Martín et al. 2011).

As a prototypical Seyfert 2 galaxy with starburst at a distance of 14.4 Mpc (1″ = 72 pc, Bland-Hawthorn et al. 1997), NGC 1068 was observed at radio (Greenhill et al. 1996), millimeter (Schinnerer et al. 2000), infrared (Jaffe et al. 2004), optical (Antonucci & Miller 1985), UV (Antonucci et al. 1994), and X-ray (Kinkhabwala et al. 2002). High spatial resolution CO (1–0) observations show two molecular spiral arms with a diameter of ∼40″ and a northern half-bar, while a CO (2–1) map reveals a nuclear ring with two bright knots in the CND region (Schinnerer et al. 2000). The dense gas fraction as traced by HCN (1–0) (Tacconi et al. 1994; Helfer & Blitz 1995) and CS (2–1) (Tacconi et al. 1997; Takano et al. 2014) in the nuclear region is higher than the two arms. Observations of CO (3–2) (Krips et al. 2011; Tsai et al. 2012; García-Burillo et al. 2014) showed that the difference of molecular gas temperatures between the nuclear region and the two arms was not as large as that of densities. Dozens of molecular lines at millimeter wavelength were detected at CND with single-dish observations (Usero et al. 2004; Nakajima et al. 2011, 2013; Aladro et al. 2013). Moreover, several molecules were detected and resolved toward NGC 1068 with interferometers in the past few years (Tosaki et al. 2017; Kelly et al. 2017; Furuya & Taniguchi 2016; Izumi et al. 2016; Imanishi et al. 2016; Nakajima et al. 2015; Viti et al. 2014; Takano et al. 2014; García-Burillo et al. 2014, 2016). The molecular gas in the CND region was denser and hotter than that in the starburst ring, while chemical properties in the two regions were also different (Viti et al. 2014). The highest molecular gas temperature was higher than 150 K, and the gas density was above 10^5 cm^{-3} in the CND region (Viti et al. 2014). The distribution of different species of molecules were also different: CO isotopic species, for instance, were enhanced in the starburst ring, while the shock/dust related molecules were enhanced in the CND region (Nakajima et al. 2015). The spatially resolved observations showed that the CND region was a complex dynamical system. For instance, the east and west

⋆ The reduced spectrum (FITS file) is only available at the CDS via anonymous ftp to cdsarc.u-strasbg.fr (130.79.128.5) or via http://cdsarc.u-strasbg.fr/viz-bin/qcat?J/A+A/613/A3

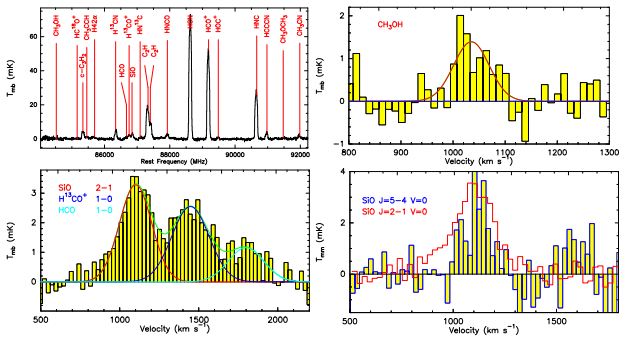

Fig. 1. *Left upper*: observed 3 mm band spectrum toward the center of NGC 1068 from 84.0 to 92.2 GHz. We mark each identified spectral line, using its rest frequency. The original RMS is about 1.50 mK at a frequency resolution of 0.195 MHz. The RMS is 0.45 mK after smoothing to the frequency resolution of 5.273 MHz at the rest frequency of 86.847 GHz. Eighteen lines were identified in this band, except for C_2H (1–0), which ranges from 87.284 to 87.447 GHz. *Right upper*: CH_3OH ($5_{-1,5}$–$4_{0,4}$) (filled yellow) and Gaussian fitting profile (red line). The RMS is 0.41 mK at a velocity resolution of 12.47 km s^{-1}. *Left lower*: SiO (2–1), $H^{13}CO^+$ (1–0), and HCO ($1_{0,1}$–$0_{0,0}$) (filled yellow), overlaid with Gaussian fitting profiles (red for SiO, blue for $H^{13}CO^+$, light blue for HCO, and green for the combination of the three components). The RMS is 0.37 mK at the velocity resolution of 24.27 km s^{-1}. *Right lower*: SiO (5–4) (blue line and filled yellow) overlaid with SiO (2–1) (red line). The RMS is 0.94 mK for SiO (5–4) at a velocity resolution of 21.85 km s^{-1}, while it is 0.32 mK for SiO (2–1) at a velocity resolution of 24.27 km s^{-1}.

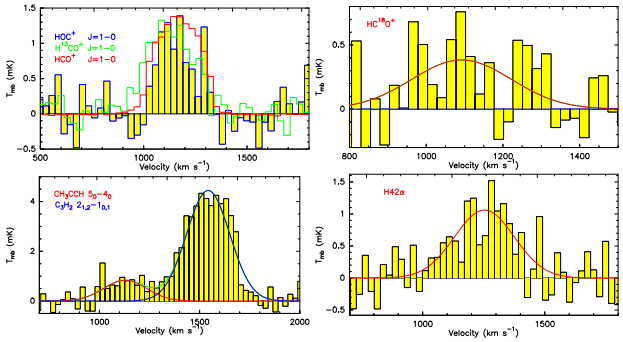

Fig. 2. *Left upper*: HOC^+ (1–0) (blue line and filled yellow) overlaid with $H^{13}CO^+$ (1–0) (green line, divided by 2), and HCO^+ (1–0) (red line, divided by 38). The RMS is 0.30 mK for HOC^+ (1–0) at a velocity resolution of 29.44 km s^{-1}. The RMS is 0.31 mK for $H^{13}CO^+$ (1–0) at a velocity resolution of 30.37 km s^{-1}. The RMS is 0.89 mK for HCO^+ (1–0) at a velocity resolution of 29.54 km s^{-1}. *Right upper*: $HC^{18}O^+$ (1–0) (filled yellow) and the Gaussian fitting profile (red line). The RMS is 0.27 mK at a velocity resolution of 24.75 km s^{-1}. *Left lower*: CH_3CCH (5_0–4_0) and c-C_3H_2 ($2_{1,2}$–$1_{0,1}$) (filled yellow), overlaid with the Gaussian fitting profiles (red for CH_3CCH, blue for c-C_3H_2, and green for the combination of the two components). The RMS is 0.36 mK at a velocity resolution of 24.67 km s^{-1}. *Right lower*: H42α (filled yellow) and Gaussian fitting profile (red line). The RMS is 0.43 mK at a velocity resolution of 24.60 km s^{-1}.

Table 1. Band parameters.

Band range GHz	EF^* GHz	$F_{\rm eff}$ %	$B_{\rm eff}$ %	HPBW $''$	Spatial resolution kpc
84.0–92.2	86	95	81	29.3–26.9	2.1–1.9
162.2–166.2	145	93	74	15.2–14.8	1.0
211.6–219.4	210	94	63	11.6–11.2	0.8
217.2–227.4	210	94	63	11.3–10.8	0.8
237.7–245.5	230	92	58	10.3–10.0	0.7

Notes. EF* means equivalent frequency, where $\frac{\rm HPBW}{\rm arcsec} = \frac{2460}{\rm Freq} \times \frac{1}{\rm GHz}$. $F_{\rm eft}$ and $B_{\rm eff}$ were taken from the web site of the IRAM 30 m. http://www.iram.es/IRAMES/mainWiki/Iram30mEfficiencies

dots were dominated by a fast shock and a slower shock (Kelly et al. 2017), while the dust torus also showed complex kinematics (García-Burillo et al. 2016). Gas inflow was driven by a past minor merger (Furuya & Taniguchi 2016), while the outflow was AGN driven (García-Burillo et al. 2014). We conducted a deeper survey of millimeter lines toward the CND region of NGC 1068 with the IRAM 30 m telescope, with the goal to quantify the gas properties in the CND. Compared to previous single-dish observations, our data probe weaker transition lines, which could place more constraints on the physical and chemistry properties of the CND.

In this paper, we focus on the transition line identification as well as on the basic physical parameter estimation. The detailed analysis for the physical and chemical properties and discussion will be the focus of a future paper. This paper is organized as follows: in Sect. 2 we present observations and data reduction, and the main results of the detected lines are provided in Sect. 3, we discuss the properties of carbon chain molecules and shock-related molecules in Sect. 4, and give a briel summary in Sect. 5.

2. Observations and data reduction

The observations toward the center of NGC 1068 (RA: 02:42:40.70 Dec: –00:00:48.0 J2000) were made at the end of December 2011, using the IRAM 30 m telescope at Pico Veleta, Spain[1]. The Eight Mixer Receiver (EMIR) with dual-polarization and the Fourier Transform Spectrometers (FTS) backend, which gave the frequency channel spacing of 195 kHz and 8 GHz instantaneous frequency coverage per sideband and per polarization, were used. The standard wobbler-switching mode with a ±120$''$ offset at 0.5 Hz beam throwing was used for the observations. Pointing was checked about every two hours with nearby strong millimeter-emitting quasi-stellar objects. The typical system temperatures were 110 K at the 3 mm band, 142 K at the 2 mm band, and 172–223 K at the 1 mm band. We read out each spectrum every 12 min, which had an effective on-source time of about 5 min.

The molecular line intensities indicated in the antenna temperature ($T_{\rm A}$) were converted into the main beam temperature ($T_{\rm mb}$) using $T_{\rm mb} = T_{\rm A} \times \frac{F_{\rm eff}}{B_{\rm eff}}$, with the parameters of each band listed in Table 1. The data were reduced with the CLASS software of the GILDAS package[2]. We inspected each spectrum visually, and qualified spectra by comparing the measured noise and the theoretical noise before and after a few times of the boxcar smoothing. None of the spectra was discarded during the qualification. We subtracted linear baselines for all spectra and averaged them with time weighting for each frequency coverage, which is listed in Table 1. We identified each line by referring to frequencies from the National Institute of Standards and Technology (NIST) database recommended rest frequencies for observed interstellar molecular microwave transitions[3].

[1] Based on observations carried out with the IRAM 30 m telescope. IRAM is supported by INSU/CNRS (France), MPG (Germany), and IGN (Spain).
[2] CLASS http://www.iram.fr/IRAMFR/GILDAS
[3] NIST http://pml.nist.gov/cgi-bin/micro/table5/start.pl

Table 2. Detected lines in NGC 1068.

Line	Frequency MHz	Flux mK km s^{-1}	Velocity km s^{-1}	Line width km s^{-1}	Tpeak mK	RMS mK
CH_3OH ($5_{-1,5}$–$4_{0,4}$)	84521.2	127.2 ± 28.0	1035.7 ± 8.9	78.0 ± 19.1	1.53	0.41
$HC^{18}O^+$ (1–0)	85162.2	125.6 ± 40.3	1124.7 ± 58.3	317.6 ± 107.9	0.37	0.27
c-C_3H_2 ($2_{1,2}$–$1_{0,1}$)	85338.9	1190.3 ± 59.9	1128.6 ± 6.3	249.6 ± 12.4	4.48	0.36
CH_3CCH (5_0–4_0)	85457.3	347.5 ± 107.2	1126.0 ± 42.4	363.8 ± 156.7	0.90	0.36
H42α	85695.0	448.2 ± 77.7	1251.0 ± 28.3	377.1 ± 91.9	1.12	0.43
$H^{13}CN$ (1–0)	86340.2	1249.8 ± 37.2	1109.6 ± 3.1	211.9 ± 7.3	5.54	0.45
HCO ($1_{0,1}$–$0_{0,0}$)	86670.8	376.9 ± 107.6	1186.4 ± 38.7	293.8 ± 86.4	1.21	0.37
$H^{13}CO^+$ (1–0)	86754.3	758.2 ± 38.7	1127.8 ± 6.9	275.5 ± 16.0	2.60	0.31
SiO (2–1)	86847.0	878.9 ± 64.5	1101.1 ± 7.8	248.5 ± 21.5	3.32	0.37
$HN^{13}C$ (1–0)	87091.0	251.5 ± 24.1	1126.9 ± 12.2	243.6 ± 24.6	0.97	0.29
HNCO ($4_{0,4}$–$3_{0,3}$)	87925.2	674.8 ± 44.6	1148.0 ± 9.0	272.9 ± 20.6	2.32	0.27
HCN (1–0)	88631.8	20754.0 ± 28.8	1155.6 ± 0.2	250.3 ± 0.4	77.91	0.44
HCO^+ (1–0)	89188.5	14519.0 ± 56.0	1167.6 ± 0.5	245.0 ± 1.0	55.66	0.89
HOC^+ (1–0)	89487.4	248.1 ± 31.9	1154.2 ± 13.5	192.8 ± 26.8	1.21	0.30
HNC (1–0)	90663.6	7835.6 ± 35.0	1185.9 ± 0.6	244.3 ± 1.2	30.10	0.39
HC_3N (10–9)	90979.0	928.5 ± 35.5	1167.6 ± 4.1	213.2 ± 9.3	4.09	0.31
CH_3OCH_3 ($3_{2,2}$–$3_{1,3}$)	91476.6	224.8 ± 52.2	1060.6 ± 49.7	410.3 ± 100.1	0.52	0.33
CH_3CN (5_0–4_0)	91987.1	395.3 ± 43.8	1196.7 ± 10.2	203.5 ± 29.6	1.82	0.35
HC_3N (18–17)	163753.4	556.4 ± 104.8	1095.8 ± 18.4	195.2 ± 40.0	2.68	1.14
SO (5_5–4_4)	215220.8	553.1 ± 82.9	1135.1 ± 16.7	210.5 ± 34.6	2.47	0.79
SiO (5–4)	217105.0	479.9 ± 81.1	1117.4 ± 11.1	137.8 ± 27.7	3.27	0.94
$C^{18}O$ (2–1)	219560.4	3438.3 ± 350.0	1105.4 ± 5.1	173.2 ± 13.8	18.70	1.80
SO (5_6–4_5)	219949.4	5070.6 ± 364.1	1217.2 ± 20.9	571.6 ± 43.7	8.33	1.80
^{13}CO (2–1)	220398.7	13314.0 ± 126.7	1134.8 ± 1.1	224.8 ± 2.3	55.60	1.80
CH_3CN (12_0–11_0)	220747.3	2084.2 ± 385.8	1132.1 ± 36.7	377.9 ± 70.1	5.18	1.80
H_2CO ($3_{1,2}$–$2_{1,1}$)	225697.8	1190.0 ± 170.6	1161.7 ± 14.8	208.3 ± 33.5	5.37	2.13
SO_2 ($14_{3,11}$–$14_{2,12}$)	226300.0	2947.8 ± 175.5	1097.9 ± 5.8	191.1 ± 12.2	14.49	2.50
CN ($2_{3/2,5/2}$–$1_{1/2,3/2}$)	226659.5	10231.0 ± 372.6	1150.3 ± 3.9	233.1 ± 8.9	41.24	2.50
CN ($2_{5/2,7/2}$–$1_{3/2,5/2}$)	226874.8	16479.0 ± 342.2	1144.7 ± 2.3	226.5 ± 4.9	68.36	2.50
HNCO ($11_{0,11}$–$10_{0,10}$)	241774.0	1602.4 ± 194.7	1121.7 ± 14.8	236.4 ± 30.6	6.37	1.66
CS (5–4)	244935.6	2703.2 ± 187.4	1148.8 ± 6.7	189.8 ± 13.9	13.38	1.88

Notes. Transition lines in boldface are new detections in NGC 1068. The parameters were obtained from Gaussian fits to the lines. Peak temperatures are given on the main-beam scale. The RMS of each line depends on the frequency resolution and the frequency selected for the calculation. The RMS shown in the last column is given to indicate the identified transition line and avoid confusion with the various RMS given in the paper. The C_2H (1 − 0) Gaussian fit parameters are not listed in this table and are described in detail in Sect. 4.

3. Results

Thirty-two lines, including 31 lines from 26 molecules and 1 hydrogen recombination line, were detected toward the nuclear region of NGC 1068. The detected C_2H (1–0) (ethynyl) lines show a double-component profile instead of six hyperfine lines due to line broadening, which were counted as one line in our list. All the detected lines are listed in Table 2, including the information of velocity-integrated fluxes, line center velocities, and line widths, which were obtained from Gaussian fitting with CLASS. Fifteen lines were first detected in NGC 1068, which are noted in Table 2 in boldface.

CH_3OCH_3 was tentatively detected as the first detection of this molecule in galaxies. The molecules, which have previously been detected in other galaxies but were detected for the first time in NGC 1068, were $HC^{18}O^+$, CH_3CCH, and H_2CO. Some molecules have previously been detected in NGC 1068 with other transitions, but the lines were first detected, such as SiO (5–4), H42α, HNCO ($11_{0,11}$–$10_{0,10}$), HC_3N (18–17), SO(5_6–4_5), and SO (5_5–4_4).

Four molecules are detected with multiple transitions, which are SiO (2–1) and (5–4), HNCO($4_{0,4}$–$3_{0,3}$) and ($11_{0,11}$–$10_{0,10}$), HC_3N(10–9) and (18–17), and CH_3CN (5_0–4_0) and (12_0–11_0). Lines of isotopic molecules are detected for four groups of molecules, which are HCO^+ (1–0), $H^{13}CO^+$ (1–0), $HC^{18}O^+$ (1–0); HCN (1–0), $H^{13}CN$ (1–0); HNC (1–0), $HN^{13}C$ (1–0); ^{13}CO (2–1), and $C^{18}O$ (2–1). The transition lines for three types of isomers are detected, which are $H^{13}CN$ (1–0) and $HN^{13}C$ (1–0), HCN (1–0) and HNC (1–0), and HCO^+ (1–0) and HOC^+ (1–0). The spectrum of each line is shown in Figs. 1 to 6.

We estimated column densities of the five newly detected species (CH_3CCH, CH_3OCH_3, H_2CO, SO_2, and $HC^{18}O^+$) toward the center of NGC 1068 under local thermal equilibrium (LTE) assumption with the following equation:

$$N = \frac{8\pi k\,\nu^2\,Q(T_{\rm ex})}{hc^3}\,A_{\rm ul}\,g_{\rm u}\,e^{E_{\rm u}/kT_{\rm ex}}\,C_\tau \int T_{MB}\,{\rm d}v, \quad (1)$$

where k is the Boltzmann constant in J K^{-1}, ν is the rest frequency of the transition line in Hz, $Q(T_{\rm ex})$ is the partition function, h is the Planck constant in J s, c is the light speed in cm s $^{-1}$, $A_{\rm ul}$ is the spontaneous emission coefficient in s^{-1}, $g_{\rm u}$ is the total degeneracy of upper energy level, $E_{\rm u}/k$ is the upper

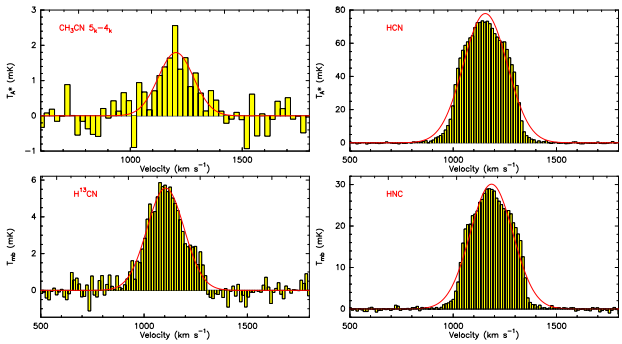

Fig. 3. *Left upper*: CN_3CN (5_k–4_k) (filled yellow) and Gaussian fitting profile (red line). The RMS is 0.40 mK at a velocity resolution of 11.89 km s^{-1}. *Right upper*: HCN (1–0) (filled yellow) and Gaussian fitting profile (red line). The RMS is 0.44 mK at a velocity resolution of 11.89 km s^{-1}. *Left lower*: $H^{13}CN$ (1–0) (filled yellow) and Gaussian fitting profile (red line). The RMS is 0.45 mK at a velocity resolution of 12.21 km s^{-1}. *Right lower*: HNC (1–0) (filled yellow) and Gaussian fitting profile (red line). The RMS is 0.39 mK at a velocity resolution of 11.62 km s^{-1}.

Table 3. Column densities.

Molecule	$N_{\rm mol}$ cm^{-2}
CH_3OCH_3	$\leq (2.3 \pm 1.4) \times 10^{15}$
CH_3CCH	$(1.4 \pm 0.9) \times 10^{15}$
H_2CO	$(7.3 \pm 12) \times 10^{13}$
SO_2	$(3.2 \pm 3.2) \times 10^{15}$
$HC^{18}O^+$	$(7.1 \pm 2.7) \times 10^{12}$

level energy in K, C_τ is the factor of optical depth correction, and $\int T_{MB}\,{\rm d}v$ is the detected transition line integrated intensity in K cm s^{-1}. The values of $Q(T_{\rm ex})$, $A_{\rm ul}$, $g_{\rm u}$, and $E_{\rm u}/k$ were taken from the Cologne Database for Molecular Spectroscopy (CDMS) catalog[4] and splatagogue astronomical spectroscopy database[5]. To simplify the problem and facilitate calculation, we assumed an average source size of 4″ for the beam dilution correction for all these five species. We used the rotational temperature of 10 ± 5 K for four species (CH_3CCH, CH_3OCH_3, H_2CO, and $HC^{18}O^+$; the explanation in Aladro et al. 2013), and 60 ± 30 K for SO_2, which is equal to the rotational temperature of SO we derived.

Since the C_2H (1–0) hyperfine transition lines are mainly optically thin (see Sect. 4 for details), the optical depth correction was not considered. The column densities of the five newly detected species are listed in Table 3.

The information of individual molecules are listed below:

– Methyl alcohol – CH_3OH
CH_3OH ($5_{-1,5}$–$4_{0,4}$) was detected at the rest frequency of 84.521 GHz in NGC 1068 (see Fig. 1). A detailed discussion of this line as a new mega-maser molecule has been presented in Wang et al. (2014a).

– Oxomethyl – HCO and silicon monoxide – SiO
HCO ($1_{0,1}$–$0_{0,0}$) was detected at the rest frequency of 86.671 GHz in this source, blended with $H^{13}CO^+$ (1–0) and SiO (2–1, v = 0) at the rest frequencies of 86.754 GHz and 86.847 GHz, respectively (Fig. 1). We used three-component Gaussian fitting to deblend the lines. Our results are consistent with the detection of this line reported in the literature (Usero et al. 2004; García-Burillo et al. 2010; Aladro et al. 2013). With about 25% noise level at same velocity resolution as in Aladro et al. (2013), we obtained reliable information for the three lines, with free parameters for Gaussian fitting instead of the fixed parameters that were used in Aladro et al. (2013).

SiO (5–4, v = 0) was also detected at the rest frequency of 217.105 GHz and is overlaid with SiO (2–1, v = 0) in Fig. 1.

– Isotopic oxomethyliums – HCO^+, $H^{13}CO^+$ and $HC^{18}O^+$ and hydroxymethylidynium – HOC^+
HCO^+ (1–0) was detected at the rest frequency of 89.189 GHz with a non-Gaussian profile in this source (see Fig. 2), which is consistent with the results in the literature (Usero et al. 2004; Krips et al. 2008; Aladro et al. 2013). As the isomer molecule of HCO^+, HOC^+ (1–0) line at the rest frequency of 89.487 GHz was also detected, which is consistent with the results in the literaure (Usero et al. 2004; Aladro et al. 2013). We overlaid HCO^+ (1–0) with $H^{13}CO^+$ (1–0), and HOC^+ (1–0) in Fig. 2.

$HC^{18}O^+$ (1–0) at the rest frequency of 85.162 GHz (Fig. 2) was marginally detected in NGC 1068. This is the third detection of this molecule in galaxies, while the first detection was $HC^{18}O^+$ (2–1) toward NGC 253 (Martín et al. 2006), and the second detection is $HC^{18}O^+$ (1–0) in M 82 (Aladro et al. 2015). We obtained the lowest column density of a molecular survey so far toward the center of NGC 1068, with $N_{HC^{18}O^+} = (7.1 \pm 2.7) \times 10^{12}$ cm^{-2}.

– Propyne – CH_3CCH and cyclopropenylidene – c-C_3H_2
CH_3CCH (5_0–4_0) and c-C_3H_2 ($2_{1,2}$–$1_{0,1}$) were detected at the rest frequencies of 85.457 GHz and 85.339 GHz. Two-component Gaussian fitting was used for these two lines, and they are overlaid with the spectrum in Fig. 2. This is the first detection of propyne in NGC 1068. Its column density is listed in Table 3. c-C_3H_2 ($2_{1,2}$–$1_{0,1}$), as a stronger line than CH_3CCH, is consistent with the detections reported in the literature (Nakajima et al. 2011).

– Hydrogen recombination lines - H42α, and acetonitrile – CH_3CN
H42α was detected at the rest frequency of 85.695 GHz (Fig. 2). The central velocity of H42α is redshifted by about 100 km s^{-1} more than most of molecular lines, which implies that the emission of H42α does not come from the same region as the molecular gas in the CND. It might be from HII regions in the arms with strong Hα emission (Scoville et al. 1988) or from the narrow-line region of central AGN. Since velocities of molecular lines, such as CS (2–1) and ^{13}CO (1–0), in spiral arms are more redshifted by about 100 km s^{-1} than those in the CND (Takano et al. 2014) and we did not detect either broad- or narrow -line emission of H26α toward the central region of NGC 1068 with ALMA (Izumi et al. 2016), we suggest that H42α more likely comes from spiral arms than from the narrow-line region of the AGN.

CH_3CN (5_k–4_k) was detected at the rest frequency of 91.987 GHz (Fig. 3), as has been reported in the literature (Aladro et al. 2013). CH_3CN (12_k–11_k) was also detected at the rest frequency of 220.747 GHz (Fig. 5).

– Isotropic hydrogen cyanides – HCN and $H^{13}CN$
HCN (1–0) was detected at the rest frequency of 88.630 GHz (Fig. 3) as the strongest line in this observation and shows a non-Gaussian profile. This line has been reported several times in the literature (Tacconi et al. 1994; Krips et al. 2008; Nakajima et al. 2011, 2013; Aladro et al. 2013). $H^{13}CN$ (1–0)

[4] http://www.astro.uni-koeln.de/cdms/catalog
[5] http://www.cv.nrao.edu/php/splat/

was detected at the rest frequency of 86.340 GHz (Fig. 3) in this source, which has been reported in Nakajima et al. (2011) and Aladro et al. (2013). Detailed discussions of the isotopic ratio and optical depth have been presented in Wang et al. (2014b).

– Isotopic hydrogen isocyanide – HNC and $HN^{13}C$
HNC (1–0) was detected at the rest frequency of 90.664 GHz, which iss consistent with the results in the literature (Aladro et al. 2013). We found that the line profile was almost symmetrical, but we were unable to fit it with a single Gaussian profile, as shown in Fig. 3. $HN^{13}C$ (1–0) was detected at the rest frequency of 87.091 GHz (see Fig. 4). Detailed discussions of $HN^{13}C$ have been presented in Wang et al. (2014b).

– Ethynyl – C_2H
C_2H (1–0) was detected with six hyperfine components, which is consistent with the results in the literature (Aladro et al. 2013). We mark the hyperfine lines from 1 to 6 in Fig. 4. However, we were unable to fit the six hyperfine lines with multiple Gaussian components because of line broadening. Thus, we counted the six hyperfine lines of C_2H as one detected line, and the integrated intensity is 7.94 ± 0.053 K km s^{-1}.

– Isocyanic acid – HNCO
HNCO ($11_{0,11}$–$10_{0,10}$) was detected at the rest frequency of 241.774 GHz. HNCO ($4_{0,4}$–$3_{0,3}$) was also detected at the rest frequency of 87.925 GHz, which has been reported in the literature (García-Burillo et al. 2010; Aladro et al. 2013). Our result for HNCO ($4_{0,4}$–$3_{0,3}$) agrees well with García-Burillo et al. (2010), while Aladro et al. (2013) gave a much lower line flux than ours. The flux in our detection is 674.8 ± 44.6 mK km s^{-1}, while it was 100 mK km s^{-1} in Aladro et al. (2013). HNCO ($11_{0,11}$–$10_{0,10}$) overlaid with HNCO ($4_{0,4}$–$3_{0,3}$) is presented in Fig. 4.

– Cyanoacetylene – HC_3N
We detected HC_3N (10–9) and HC_3N (18–17) at the rest frequencies of 90.979 GHz and 163.753 GHz, respectively. The results of our detection for HC_3N (10–9) are consistent with that in Aladro et al. (2013). HC_3N (10–9) overlaid with HC_3N (18–17) is presented in Fig. 4. The fluxes of HC_3N (18–17) and (10–9) are $\sim 3.90 \pm 0.15$ Jy km s^{-1} and $\sim 2.34 \pm 0.44$ Jy km s^{-1}, respectively.

– Dimethyl ether – CH_3OCH_3
CH_3OCH_3 ($3_{2,2}$–$3_{1,3}$) was marginally detected at the rest frequency of 91.477 GHz (Fig. 5). This is the first detection of this molecule in external galaxies. It has up to nine atoms and is the heaviest molecule detected so far with (sub-)millimeter transitions in such sources. Since it was a marginal detection, we only list an upper limit of the column density with $N_{CH_3OCH_3} = (2.3 \pm 1.4) \times 10^{15}$ cm^{-2}.

– Isotopic carbon monoxides – ^{13}CO and $C^{18}O$ and sulphur monoxide – SO
$C^{18}O$ (2–1), SO (5_6–4_5), ^{13}CO (2-1), and CH_3CN (12_0–11_0) were detected at the rest frequency of 219.560 GHz, 219.949 GHz, 220.399 GHz, and 220.747 GHz, respectively. They are blended (Fig. 5). Our results for ^{13}CO (2–1) are consistent with that in the literature (Israel 2009). In order to better show the weak lines, we first used four-component Gaussian fitting for the spectrum and then subtracted the two strong lines (^{13}CO (2–1) and $C^{18}O$ (2–1)). Then, we used a two-component Gaussian to fit the residual spectrum and obtain the information for SO (5_6–4_5) and CH_3CN (12_0–11_0). SO (5_5–4_4) was also detected at the rest frequency of 215.221 GHz. It is shown in Fig. 5 with (5_6–4_5) overlaid.

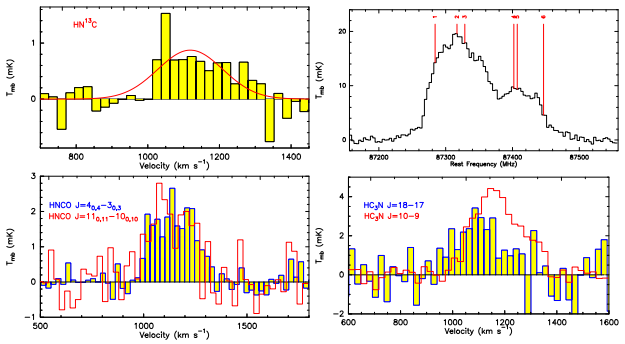

Fig. 4. *Left upper*: $HN^{13}C$ (1–0) (filled yellow) and Gaussian fitting profile (red line). The RMS is 0.29 mK at a velocity resolution of 24.20 km s^{-1}. *Right upper*: six hyperfine lines of C_2H (1–0), that is, $J = 3/2$–$1/2$ $F = 2$–1, $J = 1/2$–$1/2$ $F = 1$–0, $J = 1/2$–$1/2$ $F = 1$–0, $J = 1/2$–$1/2$ $F = 1$–0, and $J = 1/2$–$1/2$ $F = 1$–0, marked from 1–6. The RMS is 0.43 mK at a velocity resolution of 12.14 km s^{-1}. As described in Sect. 3, we only show the profile of the hyperfine lines without Gaussian fitting. *Left lower*: HNCO ($4_{0,4}$–$3_{0,3}$) (blue line and filled yellow) overlaid with HNCO ($11_{0,11}$–$10_{0,10}$) (red line, divided by 3). The RMS is 0.27 mK for HNCO ($4_{0,4}$–$3_{0,3}$) at a velocity resolution of 23.97 km s^{-1}. The RMS is 1.66 mK for HNCO ($11_{0,11}$–$10_{0,10}$) at a velocity resolution of 26.16 km s^{-1}. *Right lower*: HC_3N (18–17) (blue line and filled yellow) overlaid with HC_3N (10–9) (red line). The RMS is 1.14 mK for HC_3N (18–17) at a velocity resolution of 22.53 km s^{-1}. The RMS is 0.31 mK for HC_3N (10–9) at a velocity resolution of 23.17 km s^{-1}.

– Formaldehyde – H_2CO
H_2CO ($3_{1,2}$–$2_{1,1}$) was detected at the rest frequency of 225.698 GHz (Fig. 6). This is the first detection of formaldehyde in NGC 1068. Its column density is listed in Table 3.

– Sulphur dioxide – SO_2 and cyanogen – CN
SO_2 ($14_{3,11}$–$14_{2,12}$), CN ($2_{3/2,5/2}$–$1_{1/2,3/2}$), and CN ($2_{5/2,7/2}$–$1_{3/2,5/2}$) were detected at the rest frequency of 226.300 GHz, 226.660 GHz, and 226.875 GHz, respectively. They are blended (Fig. 6). We used a three-component Gaussian to fit the line profile. Our results for CN (2–1) are consistent with the results in the literature (Usero et al. 2004; Pérez-Beaupuits et al. 2009), which also exhibited two components.

– Carbon monosulfide – CS
CS (5–4) was detected at the rest frequency of 244.936 GHz (Fig. 6), which is consistent with the results in the literature (Martín et al. 2009; Bayet et al. 2009; Wang et al. 2011).

4. Discussion

4.1. Carbon-chain molecules

Several carbon-chain molecules, including C_2H, c-C_3H_2, HC_3N, CH_3CCH, CH_3CN, and CH_3OCH_3, were detected in NGC 1068.

C_2H and c-C_3H_2 are the most abundant molecules with two and three carbon atoms in the interstellar medium, and they both have a tight correlation with the star-forming regions behind diffuse and translucent clouds (Lucas & Liszt 2000; Gerin et al. 2011). C_2H was first detected by Tucker et al. (1974) in the Milky Way, while it was first detected in the extragalactic source M 82 by Henkel et al. (1988). Meier & Turner (2005) reported a high-resolution C_2H (1–0) observation toward the nuclear region of nearby galaxy IC 342, which showed that C_2H was abundant in the central ring and might be affected by photodissociation region (PDR) chemistry. The authors suggested that C_2H is probably abundant where C^+ and FUV photons are profuse (Meier & Turner 2005).

Owing to the line broadening, the six hyperfine components of C_2H (1–0) were in two groups. Two-component Gaussian fitting (Jiang et al. 2011) was used to obtain the line ratio of the two groups, which gave fluxes of 5.6 and 2.4 K km s^{-1}, respectively. The relative optical depth ratio probably is 4.25 : 41.67 : 20.75 : 20.75 : 8.33 : 4.25 for the six hyperfine transition lines (Tucker et al. 1974). When we assume that the six lines have the same excitation temperature and filling factors, the relative intensity ratio of the two groups is

$$\frac{(1-e^{-4.25\tau_0})+(1-e^{-41.67\tau_0})+(1-e^{-20.75\tau_0})}{(1-e^{-20.75\tau_0})+(1-e^{-8.33\tau_0})+(1-e^{-4.25\tau_0})}, \quad (2)$$

which decreases from about 2.2 to 1.0 with increasing τ_0. The measured ratio of the two groups is 2.25 ± 0.08, which means that the C_2H (1 − 0) lines are mainly optical thin.

C_2H and c-C_3H_2 are abundant in the diffuse and translucent matter (Lucas & Liszt 2000) and interstellar matter in the Galactic plane (Gerin et al. 2011). The emission line ratio of C_2H (1–0) to c-C_3H_2 ($2_{1,2}$–$1_{0,1}$) in NGC 1068 is 6.78 ± 0.34, close to the value of 7.13 ± 5.49 in the star-forming regions of M 51 (Watanabe et al. 2014). Future high-resolution observations of C_2H and c−C_3H_2 lines will be useful to understand C_2H and c−C_3H_2 chemistry in the nuclear region and the spiral arms of NGC 1068.

Figure 2 shows spectra of CH_3CCH (5_0–4_0) at the rest frequency of 85.457 GHz together with c-C_3H_2 ($2_{1,2}$–$1_{0,1}$) at the rest frequency of 85.339 GHz. c-C_3H_2 (cyclopropenylidene). With the designation c-, which means cyclic, it is the most stable molecule and has three carbon atoms and two hydrogen atoms (Spezzano et al. 2012). The rotational spectral line of c-C_3H_2 was first detected in Sgr B2 (Thaddeus et al. 1985), while the extragalactic c-C_3H_2 was first detected in M 82 (Mauersberger et al. 1991),0 which was used as a good tracer of a PDR in galaxies (Martín et al. 2006).

Interstellar methylacetylene (CH_3CCH) was first detected with the $J_K = 5_0$–4_0 transition in Sgr B2 (Snyder & Buhl 1973), and CH_3CN (methyl cyanide) was first detected with $J = 6$–5, also in Sgr B2 (Snyder & Buhl 1973), while CH_3CCH and CH_3CN were first detected in extragalactic sources in M 82 and NGC 253 with multiple transitions (Mauersberger et al. 1991). As second-generation molecules, the formation of CH_3CN was generally interpreted with the grain mantle evaporation scenario, such as for IRAS 16293-2422 (Bottinelli et al. 2004).

The line ratio R, defined as $\frac{I_{CH_3CCH(J=5-4)}}{I_{CH_3CN(J=5-4)}}$, is 0.84 ± 0.27 in NGC 1068, but is greater than 2 in M 82 and is 0.33 ± 0.07 in NGC 253 (Mauersberger et al. 1991). These results imply that the properties of large carbon chain molecules, such as CH_3CCH and CH_3CN, in the CND of NGC 1068 are more similar to the properties in NGC 253 than to the properties in M 82.

CH_3OCH_3 (dimethyl), which was first detected in Orion with multiple transitions (Snyder et al. 1974), was also detected in NGC 1068. The high column density of CH_3OCH_3 indicates that molecules with a methyl radical are enhanced in the CND region of NGC 1068, which makes this region an ideal candidate to search for large carbon molecules.

With deep observations toward the CND of NGC 1068, emissions from molecules with up to nine atoms have been detected, which means that these large molecules can survive in the CND regions even near AGN with a strong X-ray radiation field. Further high-resolution observations toward such sources with ALMA can better determine the chemical networks of these molecules, which is important for the formation of larger molecules and for comparing the astrochemical conditions of molecular gas near AGN with star-forming regions in galaxies.

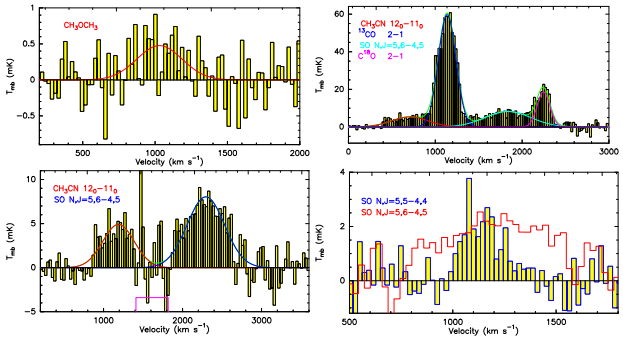

Fig. 5. *Left upper*: CH_3OCH_3 ($3_{2,2}$–$3_{1,3}$) EE (filled yellow) and Gaussian fitting profile (red line). The RMS is 0.33 mK at a velocity resolution of 23.04 km s^{-1}. *Right upper*: the four molecular transition lines (filled yellow), and their Gaussian fitting profiles, CH_3CN (12_0–11_0) (red line), ^{13}CO (2–1) (blue line), SO (5_6–4_5) (light blue), $C^{18}O$ (2–1) (pink line), and the combination of four components (green line). The RMS is 1.80 mK for ^{13}CO (2–1) at a velocity resolution of 21.52 km s^{-1}. *Left lower*: CH_3CN (12_0–11_0) (red line) overlaid with SO (5_6–4_5) (blue line). The pink window ranges the subtracted transition line ^{13}CO (2–1). Since ^{13}CO (2–1) is not a perfect Gaussian profile, some residual emission of ^{13}CO (2–1) is in the pink window. The RMS is 2.38 mK for CH_3CN (12_0–11_0) at a velocity resolution of 28.65 km s^{-1}. *Right lower*: SO (5_5–4_4) (blue line filled yellow) overlaid with SO (5_6–4_5) (red line, divided by 4). The RMS is 0.79 mK for SO (5_5–4_4) at a velocity resolution of 22.04 km s^{-1}, while it is 2.22 mK for SO (5_6–4_5) at a velocity resolution of 28.75 km s^{-1}.

4.2. Shock-related molecules

High spatial resolution of CO (3–2) observation suggests a massive molecular outflow, which was considered as a bow-shock in the molecular disk (García-Burillo et al. 2014). Lines from three shock-related molecules (SiO, SO, and HNCO) in the CND of NGC 1068 were detected with our observations. With different transitions of the fast-shock tracer SiO, the 2–1 line shows a broader line width than the 5–4 line (see Fig. 4 and Table 2), which means that part of the shocked gas was not dense enough to reach the excitation conditions of SiO (5–4). On the other hand, HNCO, which is thought to be a tracer of slow shocks or to originate from a dense region without a shock, shows similar line widths of the 11–10 and 4–3 transitions (see Fig. 15 and Table 2). High-resolution observations of the SiO and HNCO lines (García-Burillo et al. 2010; Kelly et al. 2017) show a clear difference between these tracers with different spatial distributions. Even though high-resolution observations with millimeter interferometers will be more powerful to distinguish the shock gas tracers in these galaxies, single-dish observations with multiple transitions will also be a useful tool to study the physical properties of shocked gas.

5. Summary

With deep millimeter line observations toward the nuclear region of NGC 1068 with the IRAM 30 m telescope, we detected 32 lines, 15 of which were first detected in NGC 1068. In particular, CH_3OCH_3 was first detected in galaxies. Several carbon chain molecules (C_2H, c-C_3H_2, HC_3N, CH_3CCH, CH_3CN, and CH_3OCH_3) were detected toward the nuclear region near the

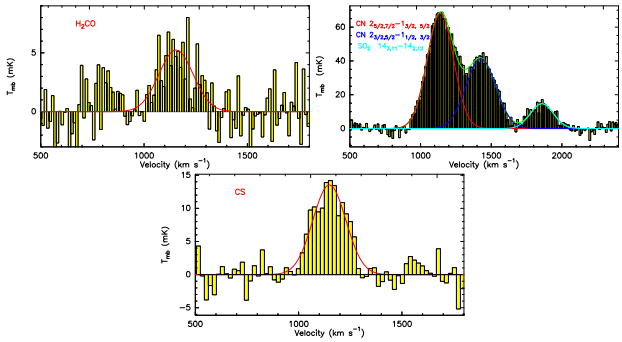

Fig. 6. *Left upper*: H_2CO ($3_{1,2}$–$2_{1,1}$) (filled yellow) and Gaussian fitting profile (red line). The RMS is 2.13 mK at a velocity resolution of 11.67 km s^{-1}. *Right upper*: all there transition lines (filled yellow), and their Gaussian fitting profiles for CN ($2_{5/2,7/2}$–$1_{3/2,5/2}$) (red line), CN ($2_{3/2,5/2}$–$1_{1/2,3/2}$) (blue line) and SO_2 ($14_{3,11}$–$14_{2,12}$) (light blue), and the combination of the three components (green line). The RMS is 2.50 mK at a velocity resolution of 11.61 km s^{-1}. *Lower*: CS (5–4) (filled yellow) and Gaussian fitting profile (red line). The RMS is 1.88 mK at a velocity resolution of 19.36 km s^{-1}.

central AGN, which needs to be explained with more chemical models for such molecular gas with a strong X-ray field. Based on the ratio of the C_2H (1–0) hyperfine features, they are optically thin. Shock-related molecules (SiO, SO, and HNCO) have also been detected with multiple transitions with different line widths, which indicates that the shocked regions had complicated excitation conditions.

Acknowledgements. We thank the anonymous referee for helpful comments for improving the paper. This work is supported by the National Key R&D Program of China (No. 2017YFA0402704), the Natural Science Foundation of China under grants of 11590783, 11473007 and 11590782. Y.S. acknowledges support from NSFC (grant 11373021). J.Q. acknowledges support from the Excellent Youth Foundation of Guangdong Province (Grant No. YQ2015128), and the Guangzhou Education Bureau (Grant No. 1201410593). We thank the staff at the IRAM 30 m telescope for their kind help and support during our observations.

References

Aladro, R., Martín, S., Martín-Pintado, J., et al. 2011, A&A, 535, A84
Aladro, R., Viti, S., Bayet, E., et al. 2013, A&A, 549, A39
Aladro, R., Martín, S., Riquelme, D., et al. 2015, A&A, 579, A101
Antonucci, R. R. J., & Miller, J. S. 1985, ApJ, 297, 621
Antonucci, R., Hurt, T., & Miller, J. 1994, ApJ, 430, 210
Bayet, E., Aladro, R., Martín, S., Viti, S., & Martín-Pintado, J. 2009, ApJ, 707, 126
Bland-Hawthorn, J., Gallimore, J. F., Tacconi, L. J., et al. 1997, Ap&SS, 248, 9
Bottinelli, S., Ceccarelli, C., Neri, R., et al. 2004, ApJ, 617, L69
Davis, T. A., Heiderman, A., Evans, N. J., & Iono, D. 2013, MNRAS, 436, 570
Furuya, R. S., & Taniguchi, Y. 2016, PASJ, 68, 103
Gao, Y., & Solomon, P. M. 2004, ApJS, 152, 63
García-Burillo, S., Usero, A., Fuente, A., et al. 2010, A&A, 519, A2
García-Burillo, S., Combes, F., Usero, A., et al. 2014, A&A, 567, A125
García-Burillo, S., Combes, F., Ramos Almeida, C., et al. 2016, ApJ, 823, L12
Gerin, M., Kaźmierczak, M., Jastrzebska, M., et al. 2011, A&A, 525, A116
Greenhill, L. J., Gwinn, C. R., Antonucci, R., & Barvainis, R. 1996, ApJ, 472, L21
Helfer, T. T., & Blitz, L. 1995, ApJ, 450, 90
Henkel, C., Schilke, P., & Mauersberger, R. 1988, A&A, 201, L23
Imanishi, M., Nakanishi, K., & Izumi, T. 2016, ApJ, 822, L10
Israel, F. P. 2009, A&A, 493, 525
Izumi, T., Nakanishi, K., Imanishi, M., Kohno, K., 2016, MNRAS, 459, 3629
Jaffe, W., Meisenheimer, K., Röttgering, H. J. A., et al. 2004, Nature, 429, 47
Jiang, X., Wang, J., & Gu, Q. 2011, MNRAS, 418, 1753
Kelly, G., Viti, S., García-Burillo, S., et al. 2017, A&A, 597, A11
Kennicutt, R. C., Jr. 1998, ApJ, 498, 541
Kinkhabwala, A., Sako, M., Behar, E., et al. 2002, ApJ, 575, 732
Krips, M., Neri, R., García-Burillo, S., et al. 2008, ApJ, 677, 262
Krips, M., Martín, S., Eckart, A., et al. 2011, ApJ, 736, 37
Liu, L., Gao, Y., & Greve, T. R. 2015, ApJ, 805, 31
Lucas, R., & Liszt, H. S. 2000, A&A, 358, 1069
Martín, S., Mauersberger, R., Martín-Pintado, J., Henkel, C., & García-Burillo, S. 2006, ApJS, 164, 450
Martín, S., Martín-Pintado, J., & Mauersberger, R. 2009, ApJ, 694, 610
Martín, S., Krips, M., Martín-Pintado, J., et al. 2011, A&A, 527, A36
Mauersberger, R., Henkel, C., Walmsley, C. M., Sage, L. J., & Wiklind, T. 1991, A&A, 247, 307
Meier, D. S., & Turner, J. L. 2005, ApJ, 618, 259
Nakajima, T., Takano, S., Kohno, K., & Inoue, H. 2011, ApJ, 728, LL38
Nakajima, T., Takano, S., Kohno, K., & line survey Team 2013, New Trends in Radio Astronomy in the ALMA Era: The 30th Anniversary of Nobeyama Radio Observatory, 476, 299
Nakajima, T., Takano, S., Kohno, K., et al. 2015, PASJ, 67, 8
Omont, A. 2007, Rep. Prog. Phys., 70, 1099
Pérez-Beaupuits, J. P., Spaans, M., van der Tak, F. F. S., et al. 2009, A&A, 503, 459
Sanders, D. B., Scoville, N. Z., & Soifer, B. T. 1991, ApJ, 370, 158
Schinnerer, E., Eckart, A., Tacconi, L. J., Genzel, R., & Downes, D. 2000, ApJ, 533, 850
Scoville, N. Z., Matthews, K., Carico, D. P., & Sanders, D. B. 1988, ApJ, 327, L61
Snyder, L. E., & Buhl, D. 1973, Nat. Phys. Sci., 243, 45
Snyder, L. E., Buhl, D., Schwartz, P. R., et al. 1974, ApJ, 191, L79
Spezzano, S., Tamassia, F., Thorwirth, S., et al. 2012, ApJS, 200, 1
Tacconi, L. J., Genzel, R., Blietz, M., et al. 1994, ApJ, 426, L77
Tacconi, L. J., Gallimore, J. F., Genzel, R., Schinnerer, E., & Downes, D. 1997, Ap&SS, 248, 59
Takano, S., Nakajima, T., Kohno, K., et al. 2014, PASJ, 66, 75
Thaddeus, P., Vrtilek, J. M., & Gottlieb, C. A. 1985, ApJ, 299, L63
Tosaki, T., Kohno, K., Harada, N., et al. 2017, PASJ, 69, 18
Tsai, M., Hwang, C.-Y., Matsushita, S., Baker, A. J., & Espada, D. 2012, ApJ, 746, 129
Tucker, K. D., Kutner, M. L., & Thaddeus, P. 1974, ApJ, 193, L115
Usero, A., García-Burillo, S., Fuente, A., Martín-Pintado, J., & Rodríguez-Fernández, N. J. 2004, A&A, 419, 897
Viti, S., García-Burillo, S., Fuente, A., et al. 2014, A&A, 570, A28
Wang, J., Zhang, Z., & Shi, Y. 2011, MNRAS, 416, L21
Wang, J., Zhang, J., Gao, Y., Zhang, Z.-Y., Li, D., Fang, M., Shi, Y., 2014a, Nat. Commun., 5, 5449
Wang, J., Zhang, Z.-Y., Qiu, J., et al. 2014b, ApJ, 796, 57
Watanabe, Y., Sakai, N., Sorai, K., & Yamamoto, S. 2014, ApJ, 788, 4
Young, J. S., & Scoville, N. Z. 1991, ARA&A, 29, 581